ADVANCED ENERGY & SUSTAINABILITY RESEARCH
Open Access
www.advenergysustres.com

Direct Electrochemical Storage of Solar Energy in C-Rich Polymeric Carbon Nitride Cell

Lirong He, Xiao Tang, Yanhong Li, Ling Zhang, and Guozhong Cao**

Covalent carbon nitrides (CNs) have been widely used in photocatalysis and energy storage for their graphitic 2D structure and semiconducting properties. However, carbon nitrides, normally with a bandgap of 2.7 eV, can absorb only the ultraviolet and blue fraction of solar spectrum ($\lambda < 450$ nm), limiting their performance in photovoltaic applications. Herein, a carbon-rich polymeric carbon nitride (CPCN) with an optical bandgap of 1.74 eV and significant absorption to the visible light (550–700 nm) is reported. The dark blue CPCN serving as the photoelectrode in a monolithic photoelectrochemical solar cell successfully demonstrates direct solar-to-electric energy conversion and storage in one single material. Under the irradiation of simulated AM1.5 solar light, the cell generates a short-circuit photocurrent density (J_{sc}) of 1.3 mA cm^{-2} and open-circuit photovoltage (V_{oc}) of 500 mV. The increase in the charge capacity of the cell has a linear dependence with the power of the incident light and the maximum specific charge capacity of 4.77 C g^{-1} is obtained. The transmission electron microscopy (TEM), X-ray diffraction (XRD), X-ray photoelectron spectroscopy (XPS), and Fourier infrared spectroscopy (FTIR) as well as photoelectrochemical measurements reveal the underlying mechanism of the observed light-induced charge storage of the CPCN.

1. Introduction

In recent years, covalent carbon nitrides (CNs) have attracted great attention, due to their unique properties, such as 2D graphitic microstructure, semiconducting properties,[1] low cost, nontoxicity, superior thermal physicochemical stability,[2] easy synthesis, and modification.[3] Since the first report in 2009,[4] CNs have been widely applied in photocatalysis,[5] adsorbents,[6] supercapacitors,[7,8] solar cells,[9,10] lithium- or sodium-ion batteries,[11] and fuel cells.[12] The basic structural unit of CNs is either triazine or heptazine cores, both of which are planar, so that the polymerized final products can be layered structure, and thus called "graphitic" carbon nitrides.[13] Continuous repetition of heptazine motifs normally leads to a bandgap of 2.7 eV.[14] This wide bandgap means that it can absorb only the ultraviolet and blue fraction of solar spectrum ($\lambda < 450$ nm), which limits its performance in photocatalytic and photovoltaic applications. Great efforts have been made to tune the band structure of CNs. It has been found that the lone pair electrons of N participating with the π-conjugated system of heptazine motifs can extend the conjugated backbone and thus reduce the bandgap significantly. Mane et al. demonstrated a narrow bandgap of 2.2 eV owing to the 1,2,4-triazole moiety linked to the heptazine motif.[15] Kumar et al. reported an extended conjugation due to two heptazine units being bridged together with azo linkage, which led to a bandgap of 1.76 eV.[16] Talapaneni et al. reported the 1,2,4-triazine or 1,2,4,5-tetrazine moieties being bridged together by tertiary nitrogen, i.e., N-$(C)_3$, resulted in the bandgap decrease to 2.25 eV.[17] Carbon-rich CNs network also facilitates bandgap narrowing as well as efficient charge separation due to the extended conjugated network. A C-rich C_3N_4 materials (CCN) synthesized using melamine and glucose through hydrothermal methods by Zhang at al. obtained a narrow bandgap of 2.0 eV and exhibited enhancement of photocurrent and photocatalytic activity.[18] Fang et al. synthesized a 2D carbon-rich graphitic carbon nitride (Cco-C_3N_4) through cocrystallization of terephthalic acid with melamine, which decreased the bandgap to 2.55 eV and extended the light absorption to 600 nm wavelength. They also found that the ordered carbon-rich frameworks facilitated photogenerated carrier separation and transport.[19]

In this work, a carbon-rich polymeric carbon nitrides (CPCNs) are synthesized by the hydrothermal treatment of the mixture of citric acid ($C_6H_8O_7$) and urea (CH_4N_2O), followed with aging at room temperature (≈25 °C) for an extended period of time. Owing to the narrow bandgap of 1.74 eV and the 2D conjugation of the N-bridged heptazine backbone, the resultant dark blue C-rich carbon nitride achieves intriguing photoinduced charging

L. He, X. Tang, Y. Li, L. Zhang
School of Science
Chongqing University of Posts and Telecommunications
Chongqing 400065, P. R. China
E-mail: tangxiao@cqupt.edu.cn

G. Cao
Materials Science and Engineering
University of Washington
Seattle, WA 98195-2120, USA
E-mail: gzcao@u.washington.edu

The ORCID identification number(s) for the author(s) of this article can be found under https://doi.org/10.1002/aesr.202100111.

DOI: 10.1002/aesr.202100111

and discharging, which is crucial to harvest, store, and release solar energy in the form of electrical energy.

2. Results and Discussions

When citric acid was mixed with urea by a mass ratio of 1.95 to undergo hydrothermal reaction at 200 °C for 3 h, the resulted precursor was a yellow solution. The precursor was then aged at the room temperature (≈25 °C) for different periods of time. The color of the solution changed from yellow via green into eventually dark blue in a few days (**Figure 1**a). The dark blue would not change in months. The transmission electron microscopy (TEM) images of the samples revealed the microstructure evolution of the samples with prolonging aging time. In the 4 –h aging sample (yellow), lots of ultrathin 2D nanosheets were found (Figure 1b). When the color of the sample turned into green by aging for 2 days, we found some vesicular spheres with all kinds of sizes, which were hollow or stuffed but their fine structure was indistinct (Figure 1c). Keep aging the sample at the room temperature for 35 days, we still found some spheres but with a rough surface. And it is intriguing that they have porous inner structure, which are apparently 3D nanomeshes constructed by 2D networks (Figure 1d).

The resultant products were freeze-dried and characterized by means of X-ray diffraction (XRD), X-ray photoelectron spectroscopy (XPS), and Fourier infrared spectroscopy (FTIR). The XRD patterns of samples aging for 4 h, 2 days, and 35 days show some short diffraction peaks, indicating the poor crystallinity of the sample (**Figure 2**a). The characteristic diffraction peaks of heptazine-based carbon nitrides (CNs) are visible. The peak at 13.0° corresponding to the (100) plane is specific to in-plane structural packing of heptazine units with a planar distance of $d = 0.680$ nm.[20] Diffraction peak at 27.0° corresponding to the (002) plane is attributed to the interlayer stacking of CN heterocycles with a distance of $d = 0.325$ nm.[21] It is noticeable that with the aging time prolonging from 2 days to 35 days, the peak at 27.0° becomes much weaker, indicating that the heptazine motifs change their layer-by-layer stacking mode. On the contrary, instead of getting higher and sharper, the diffraction peak at 13.0° is slightly shorter and broader, which suggests the heptazine motifs stop extending in one plane either. Except for layer-by-layer and planer extending, the 2D structure could only stack by intersectional way. That, to some extent, explained the morphology of 3D nanomesh with thin walls shown in TEM pictures (Figure 1d). The diffraction peak at 10.4° can be attributed to the characteristic (002) plane of graphene oxide (GO) sheets, corresponding to an interlayer spacing of 0.830 nm.[22] The peak at about 25.0° is indicative of the existence of π–π stacking graphene (GR) sheets with an interlayer spacing of 0.360 nm.[23] A bunch of peaks at 17.9°, 20.5°, 22.32°, 23.06°, 24.08°, and 34.22°, referring to PDF#45–1540, can be indexed to (012), (121), (112), (130), (040), and (151) crystal planes of ammonium citrate (AC), which is a by-product of residual citric acid reacting with ammonia from pyrolysis of urea during the hydrothermal process.

FTIR spectra of samples with different aging time (4 h, 2 days, and 35 days) show no significant difference and demonstrate the characteristic peaks of graphitic carbon nitrides (Figure 2b). The bending vibration of triazine rings is quite pronounced at 770 cm^{-1}[24] and the typical stretching vibration of —C—N in heterocycles in a range of 1179–1542 cm^{-1}[25] is visible. The

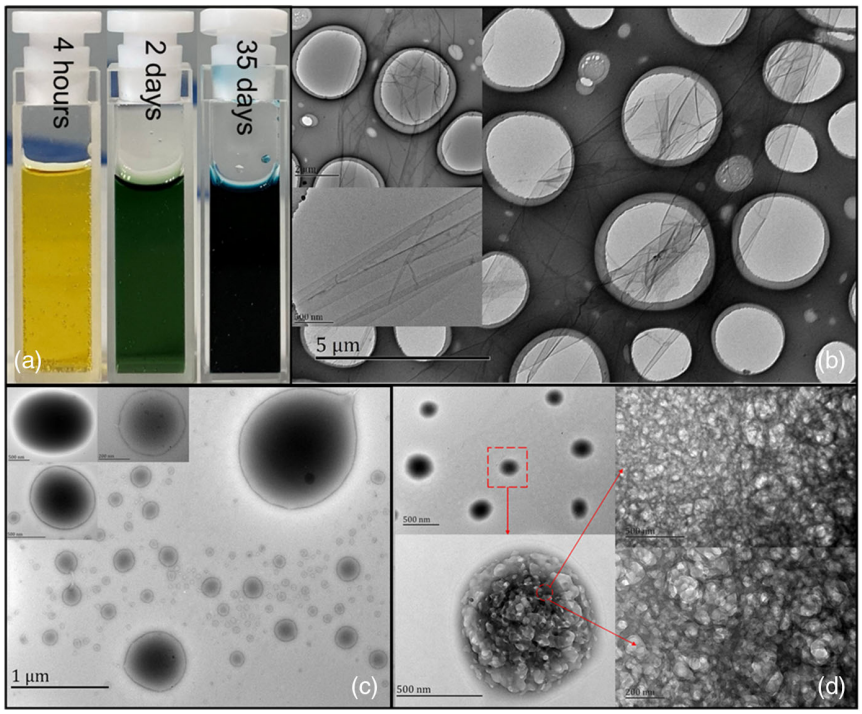

Figure 1. a) Pictures of the hydrothermal reaction product aged for 4 h (yellow), 2 days (green), and 35 days (dark blue); TEM images of the samples in different aging time: b) 4 h, c) 2 days, and d) 35 days.

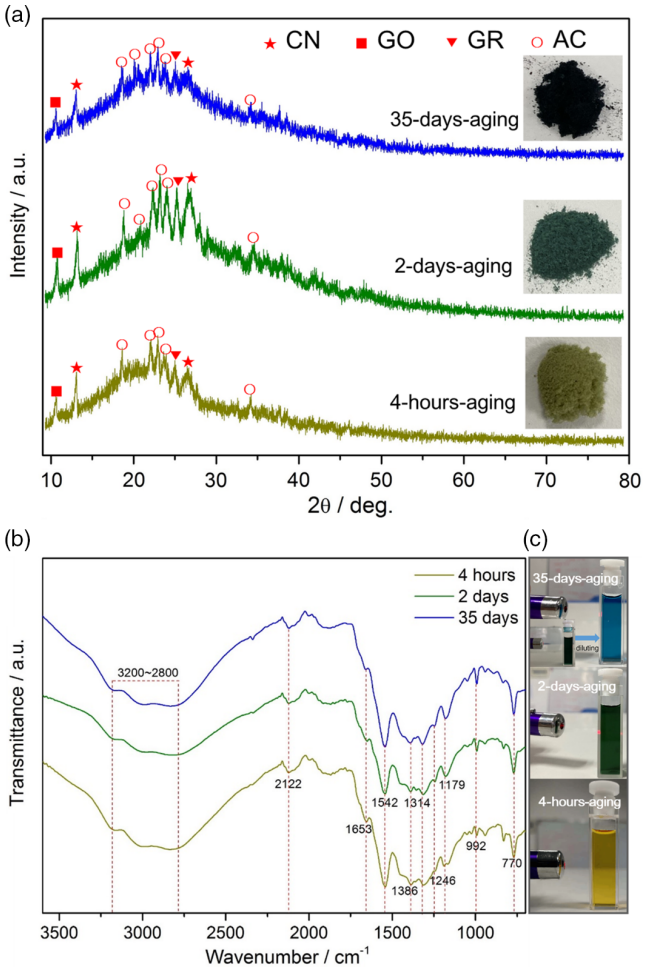

Figure 2. a) XRD patterns of the samples aging for 4 h, 2 days, and 35 days (the inset is the pictures of the corresponding frozen-dried samples), in which CN, GO, GR, and AC refer to carbon nitride, graphene oxide, graphene, and ammonium citrate, respectively; b) FTIR spectra of the samples aging for 4 h, 2 days, and 35 days, frozen-dried; c) Tyndall effects testing of the aqueous solutions of the samples.

broad absorption at 2800 cm^{-1} is attributed to N—H stretching and hydrogen-bonding interactions.[26] In addition, the peak at 992 cm^{-1} is assigned to the C—N in-plane stretching, indicating the introduction of nitrogen in the graphitic domains.[27] The peak at 2122 cm^{-1}, referring to the reference,[28] is ascribed to H—N— $(C)_2$ functional groups. The FTIR spectrum of the sample still shows some characteristic bands of surface oxidized groups, at 1653 cm^{-1} (C═O stretching vibrations) and at 1386 cm^{-1} (C—OH stretching vibrations).[29] And the stretching vibration of O—H groups in the surface adsorbed water molecules is visible at 3200 cm^{-1}.[30] The samples are soluble. When the dry samples dispersed in water, no Tyndall effects showed (Figure2c), indicating that it formed aqueous solutions rather than suspensions. Based on the aforementioned analysis, the samples should be carbon-rich polymeric carbon nitride materials with hydroxylated surfaces.

XPS survey spectra of the samples with different aging time (4 h, 2 days, and 35 days) are shown in **Figure 3**a. The pronounced peaks of C1*s* at ≈284 eV and N1*s* ≈400 eV are visible. During 35 days of aging, the N/C atomic ratio has fluctuated slightly in the range of 0.18–0.21 (the inset of **Figure 4**a), indicating the number of N atoms introduced to the graphitic carbon plane is hardly affected by aging. The C 1*s* spectrum can be deconvoluted into three peaks (Figure 3b). The peak at 284.6 eV is assigned to sp^2-bonded carbon in C—C,[31] which is symmetrical and with intensity higher than other two peaks, proving the existence of graphitic domains. The peak at 288.4 eV is identified as sp^2-bonded carbon in heptazine rings (C═N—C) and the peak at 286.8 eV is assigned to sp^3-bonded C—N.[32] The N 1*s* spectrum was deconvoluted into three peaks (Figure 3c). The peak at 398.8 eV originates from sp^2-hybridized N in heptazine rings (C═N—C).[33] The peak at 399.7 eV is assigned to sp^3-hybridized N, bridging nitrogen atom in N—$(C)_3$ or H—N—$(C)_2$ groups.[34] The peak at 400.8 eV is due to the presence of residual amino functional groups (C—NH_x).[35] The deconvoluted peak of the sp^3-hybridized N (399.7 eV) of the 35 days aged sample has higher intensity than those aged for a shorter time. Similar result is found for the sp^3-bonded C—N (286.8 eV) on the C 1*s* spectra. Those results indicate that the content of bridging N increased with prolonged aging time, implying the heptazine motifs underwent polycondensation at the room temperature. In addition, the peak intensity of O 1*s* at ≈531 eV is quite high in the survey spectra. It originated from the surface oxidized groups (Figure 3 d), such as C═O (531.1 eV) and C—OH (532.9 eV),[36] and the surface adsorbed water molecules (532.1 eV),[37] corroborating well with FTIR spectra. The high content of C═O could be the residual functional group from citric acid, one of the reactants. The XRD, FTIR, and XPS spectra suggest a hybrid structure of heptazine motif with oxidized GR. Figure 3e shows the possible four types of bonding configurations of N atoms within the C-rich carbon nitride polymer, which are sp^2-bonded N in heptazine rings (C═N—C), sp^3-hybridized N in N—$(C)_3$ groups or in H—N—$(C)_2$ groups, and residual amino functional groups (C—NH_x). Heptazine unites are connected by the bridging N in the form of N— $(C)_3$ or H—N—$(C)_2$.

The UV–vis transmittance spectrum of the 35 days aged sample reveals its significant absorption at 550–700 nm (Figure 4a). This dark blue product, with the strong optical absorption peak at 638 nm (Figure 4b), has a maximum molar extinction coefficient ($\varepsilon_{638\ nm}$) of 130.71 L mol^{-1} cm^{-1}. The $\varepsilon_{638\ nm}$ values are 4.35 and 13.67 L mol^{-1} cm^{-1} for the 4 h aging sample and the 2 days aging sample, respectively (**Figure 5**a). Based on the Tauc plots, the optical gap energy (E_g) values of 1.74, 2.71, and 3.05 eV were obtained, corresponding to the optical absorption in 550–700 nm, 400–500 nm, and less than 400 nm wavelength ranges, respectively (Figure 4c). The 35 days aged sample has a significant absorption to the visible light of 550–700 nm, owing to the significant optical bandgap of 1.74 eV. The photoluminescence (PL) spectra of the samples show noisy weak light emission signals at the wavelength range of 500–800 nm. The 35 days aged sample demonstrates less emission (Figure 4d). The combination of strong light absorption and weak fluorescence emission makes the dark blue sample a good candidate for photoelectric conversion applications.

Using TiO_2 as an electron transporter, the photoelectrode consists of CPCN and TiO_2 layered on a FTO substrate (Figure S1a, Supporting Information). The counter electrode is a platinum-

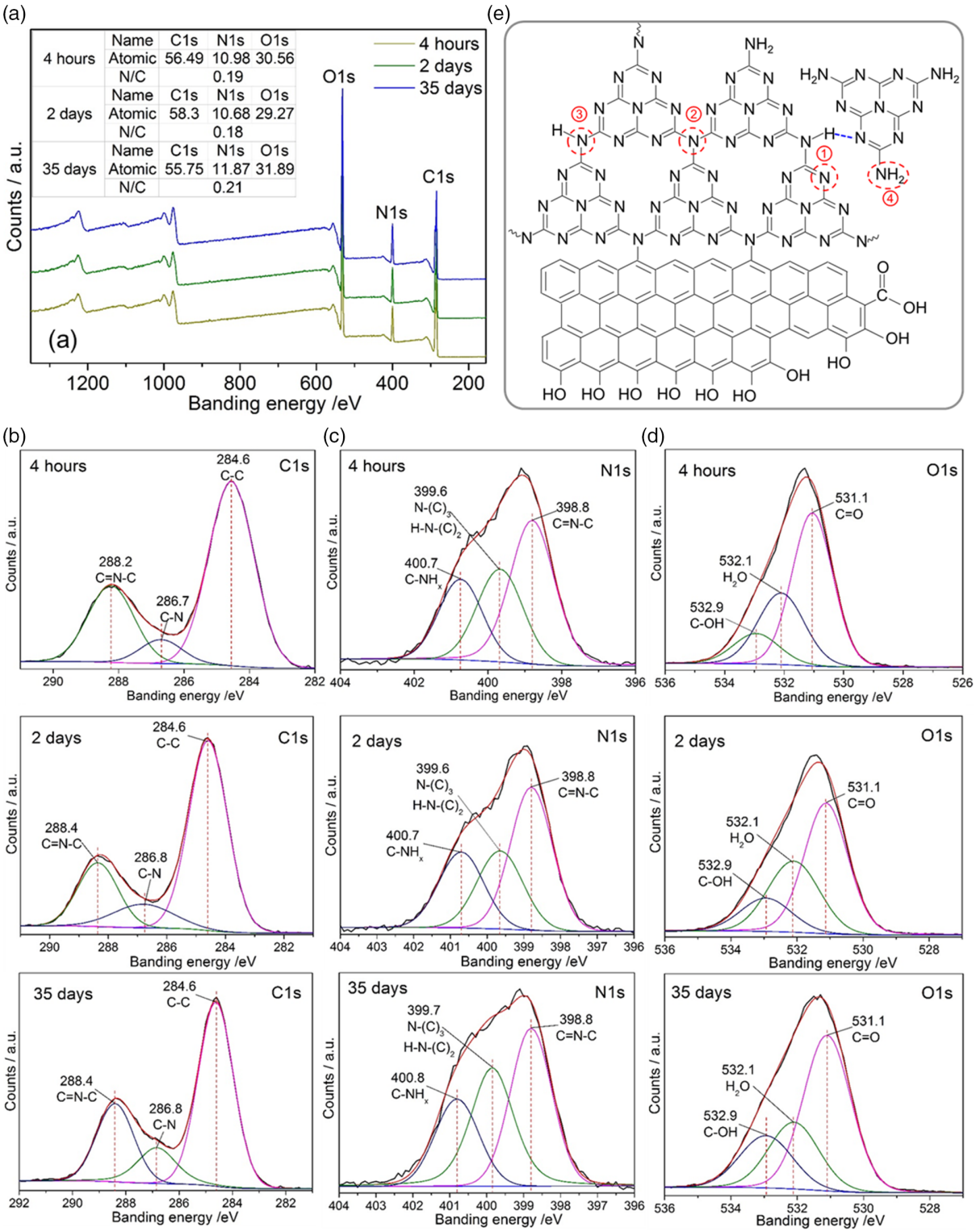

Figure 3. a) XPS survey spectra of the samples in different aging time (the inset is the corresponding atomic percentage of C, N, and O; high-resolution XPS spectra of b) C 1s, c) N 1s, d) O 1s; e) schematic structure of CPCN and the types of bonding configurations of N atoms: ① sp^2-hybridized N in heptazine rings (C═N—C); ② bridging nitrogen atoms in N—$(C)_3$ groups; ③ bridging nitrogen atoms in H—N—$(C)_2$ groups; ④ residual amino functional groups (C—NH_x).

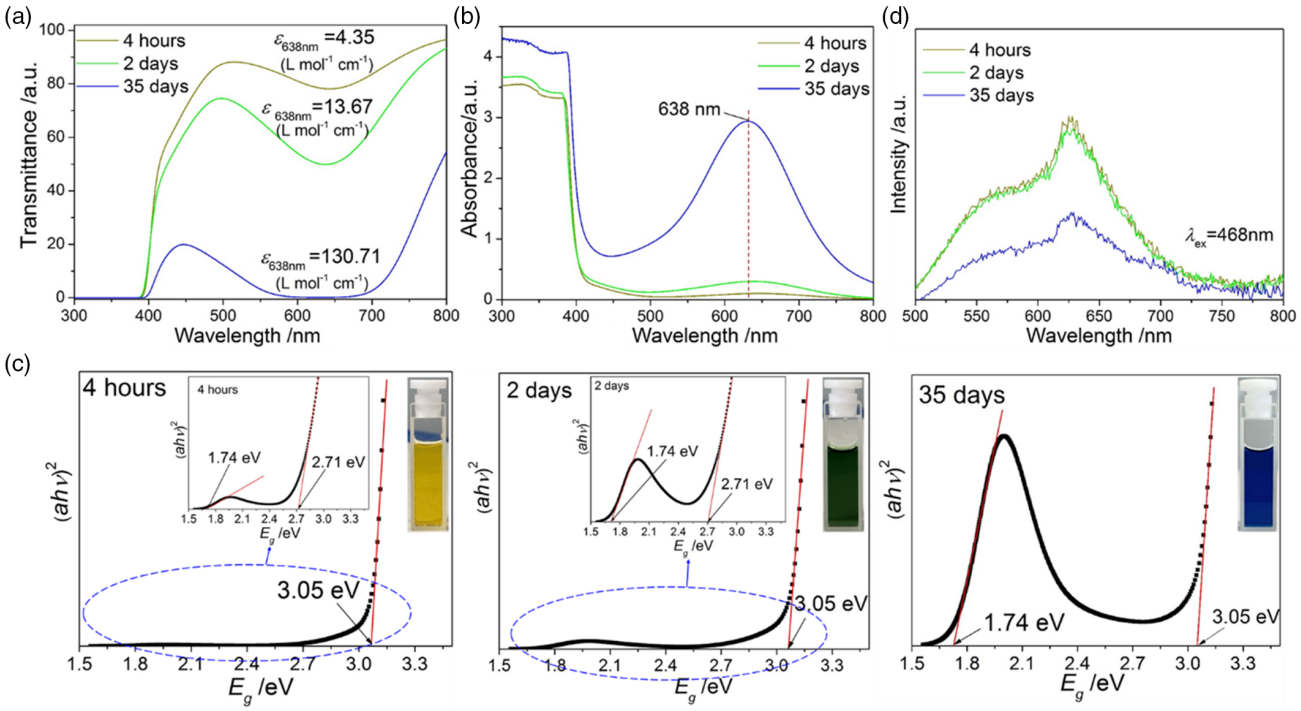

Figure 4. a) UV–vis transmittance spectra of the samples in different aging time and their maximum molar extinction coefficients at 638 nm; b) the corresponding UV–vis absorption spectra; c) Tauc plots and the corresponding optical gap energy (E_g) of the of the samples in different aging time; d) PL spectra of the samples in different aging time.

coated FTO glass. The electrolyte, using I_3^-/ I^- redox couple and the solvent of acetonitrile with hint of water ($V_{acetonitrile}$/ V_{water} = 10:1), serves as the redox shuttle. The photocurrent density J as a function of forward bias voltage V (J–V curves) of the CPCN-based photoelectrochemical solar cells under the irradiation of simulated AM1.5 solar light (100 mW cm^{-2})at the room temperature was measured, as shown in Figure S1b, Supporting Information. The I–V characteristics of the cell under illumination, which are quite different from a conventional solar cell, are discussed in the Supporting Information.

The charge storage properties of the fabricated CPCN-based cell were investigated by cyclic voltammetry (CV) and galvanostatic charge–discharge (GCD) tests. The electrochemical experiments undertook in the two-electrodes mode (Figure 5a). The CV curves were tested in a potential range of 0–1 V in dark or under the simulated solar irradiation. Under illumination, when the cell is scanned with a forward bias voltage from 0 to 490 mV, the cell generates a negative current forming a J–V curve of photoelectric conversion with J_{sc} = 0.42 mA cm^{-2} and V_{oc} = 490 mV. With the voltage increasing, the current becomes positive and an oxidation peak at 700 mV emerges, attributing to I^- being oxidized into I_3^- in the electrolyte, which is an efficient way to withdraw the holes produced by photoexcitation of the CPCN. As the voltage scans back from 1 to 0 V, attributing to the electrons withdrawn from the counter electrode by the reduction of I_3^- into I^- in the electrolyte, the cell generates an obvious negative current peak at 490 mV (Figure 5b). And with the scan rates increasing from 10 to 100 mV s^{-1}, the shape of the CV curves does not change significantly (Figure 5c). In dark, the reversible redox peaks are invisible on the CV curves, as shown in Figure 5b,d. In addition, there are also surface capacitances in the CPCN electrode, as shown on the CV curve in 600–900 mV potential range (both in dark and under illumination). Figure 5e shows the dependence of specific charge capacity of the cell on scan rates. Under illumination, with the scan rate increasing from 10 to 100 mV s^{-2}, the specific charge capacity decreases from 4.59 to 1.43 C g^{-1}, resulting in a rate capability of 31%. In dark, the cell has lower capacity of 1.82 C g^{-1} down to 0.83 C g^{-1}, but better rate capability of 0.46%. The GCD was tested at a current density of 0.4 mA cm^{-2} and in a potential window of 0–0.9 V. As shown in Figure 5f, under illumination, the charging and discharging performance of the cell is significantly enhanced. The calculated coulombic efficiency values are 0.82 and 0.50 for the cell under illumination and in dark, respectively. Under illumination, with the cycle times increasing, the CV curves in 20 cycles show a visible shift of the oxidation peak from 700 to 590 mV, while the position of reduction peak is unchanged (Figure 5g). This might result from the increase in intermediate radical species $I_2^{-\cdot}$, which exhibits a more negative redox potential than the corresponding standard redox potential of I_3^-/I^-.[38] In dark, the CV curves does not change at all (Figure 5h).

The photoelectrode with TiO_2 or CPCN alone coated on the FTO glass (denoted as TiO_2 electrode and CPCN electrode, respectively) and compared their photoelectrochemical properties with that of the CPCN/TiO_2 electrode. Figure S2a–d, Supporting Information, shows the photoelectric conversion performance (I–V), the charge storage performance (GCD) and the CV properties tested in dark and under illumination. It turns out

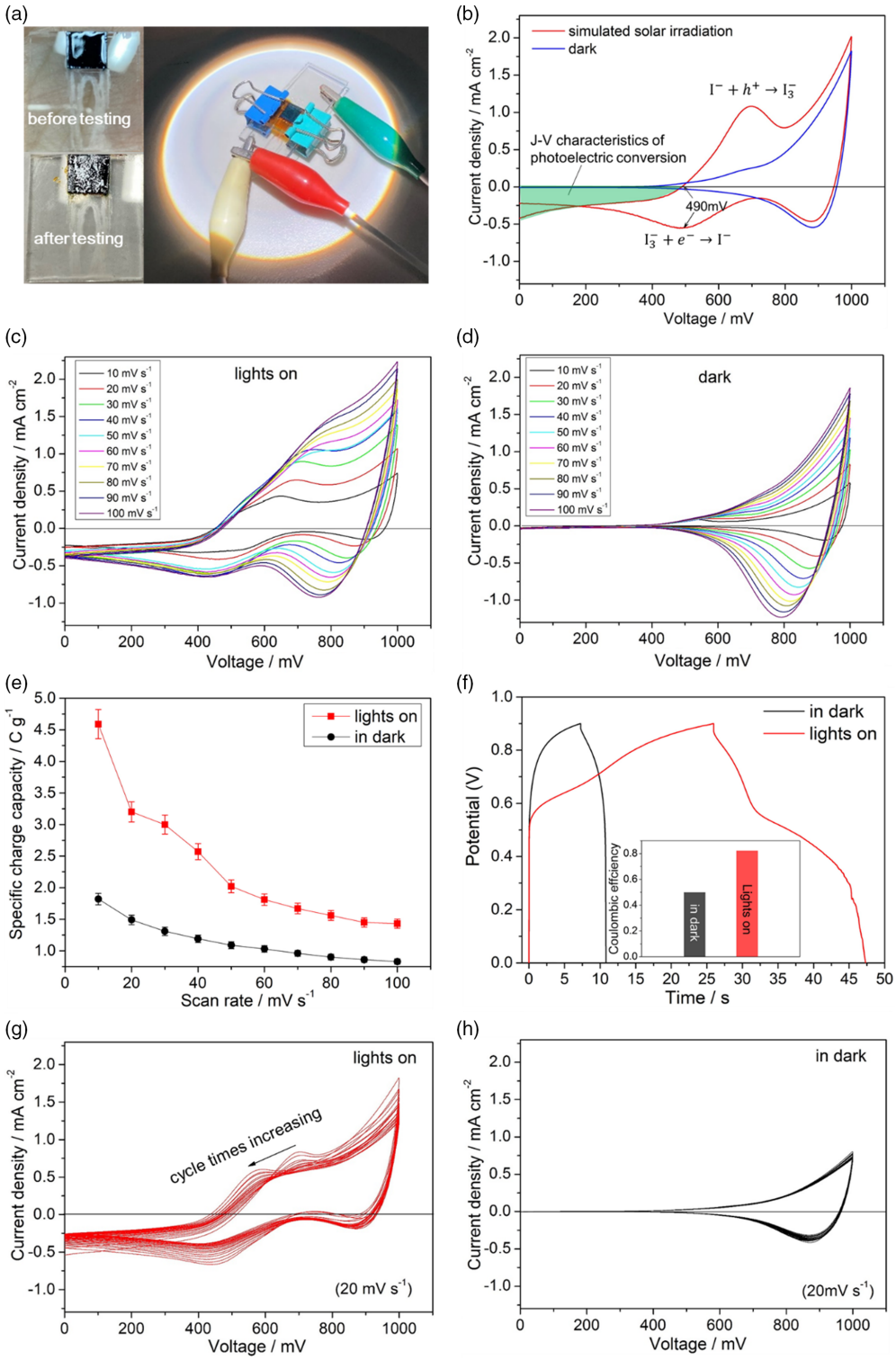

Figure 5. a) Pictures of the cell during the photoelectrochemical testing (right) and the photoelectrode before/after testing (left); b) CV curves of the CPCN-based cell tested in a potential range of 0–1 V at the scan rates of 50 mV s^{-1} in dark or under the simulated solar irradiation (150 mW cm^{-2}); CV curves of the cell tested in a potential range of 0–1 V at the different scan rates from 10 to 100 mV s^{-1} c) under the simulated solar irradiation (150 mW cm^{-2}) or d) in dark; e) specific charge capacity of the cell; f) GCD tests of the cell tested in dark or under illumination (150 mW cm^{-2}) at a current density of 0.4 mA cm^{-2} and in a potential window of 0–0.9 V (the inset is the calculated coulombic efficiency of the cell); CV curves of the cell tested g) under illumination (150 mW cm^{-2}) or h) in dark at a scan rate of 20 mV s^{-1} in 20 cycles.

that both TiO_2 electrode and CPCN electrode show poor performance. It suggests that without TiO_2 as the electron transporter, the CPCN cell will lose the photoinduced charge storage behavior.

The photoelectrochemical experiments demonstrate that the system with CPCN serving as light absorber, TiO_2 as an electron transporter, and I_3^-/I^- as hole extractor successfully constructs an efficient photoinduced charge storage regime. The band relationship of TiO_2, CPCM, and the I_3^-/I^- redox couple reveals the underlying working mechanism of the CPCN cell.

TiO_2 has a conduction band (E_c) and valence band (E_v) at −0.25 and 2.95 eV (vs E_{NHE}) or at −4.21 and −7.42 eV (vs E_{vac}), respectively.[39] The redox potential (E_{red}) of I_3^-/I^- is 0.35 V (vs E_{NHE}) or −4.92 eV (vs E_{vac}) in acetonitrile.[40] The highest occupied molecular orbital (HOMO) E_{HOMO} of the CPCN was estimated by ultraviolet photoelectron spectroscopy (UPS). **Figure 6**a shows the UPS spectra of the CPCN thin film. The high binding energy cutoff (E_{cutoff}) of the CPCN determined by linear extrapolation to zero of the yield of secondary electrons is 18.31 eV (as shown in Figure 6b). The HOMO region (0–4 eV) for the CPCN thin film is shown in Figure 6c. From the data in Figure 6c, the excitation onset energy $E_{onset} = 3.02$ eV for the CPCN. The HOMO energy is thus obtained directly from the UPS experiments by the relationship of the incident photon energy ($h\nu = 21.2$ eV), E_{cutoff} and E_{onset}[41–43]

$$E_{HOMO} = h\nu - (E_{cutoff} - E_{onset}) \quad (1)$$

For the CPCN thin film, E_{HOMO} was calculated to be −5.91 eV. The LUMO energy is calculated using the HOMO levels and the optical gaps ($E_g = 1.74$ eV) obtained from the UV–vis absorption spectra, as shown in Figure 4c. Thus, the $E_{LUMO} = -4.17$ eV is for the CPCN material.

The schematic diagram for energy levels and approximate redox potentials of TiO_2, CPCN, and I_3^-/I^- (Figure 6d) demonstrates an effective electron transfer path from the LUMO of CPCN to the conduction band of TiO_2 and the hole extract route from the HOMO of CPCN to the E_{redox} of I_3^-/I^-. Figure 6e shows the schematics of possible charging and discharging processes in the CPCN-based cell. Upon photon excitation of CPCN, the photogenerated holes were withdrawn by I^- and transferred to the counter electrode, while most photoelectrons were accumulated in CPCN to charge the cell. When discharging, the electrons stored in CPCN injected into the conduction band of TiO_2 and then transported to the external circuit through FTO conducting substrate. The electron injection from CPCN to TiO_2 was on the path of discharging, which meant there was a competition between the photoelectrons being stored and transporting under illumination. According to the *J*–*V* test results in Figure S1, Supporting Information, at the early illuminating time, the photoelectric conversion mainly happened. With

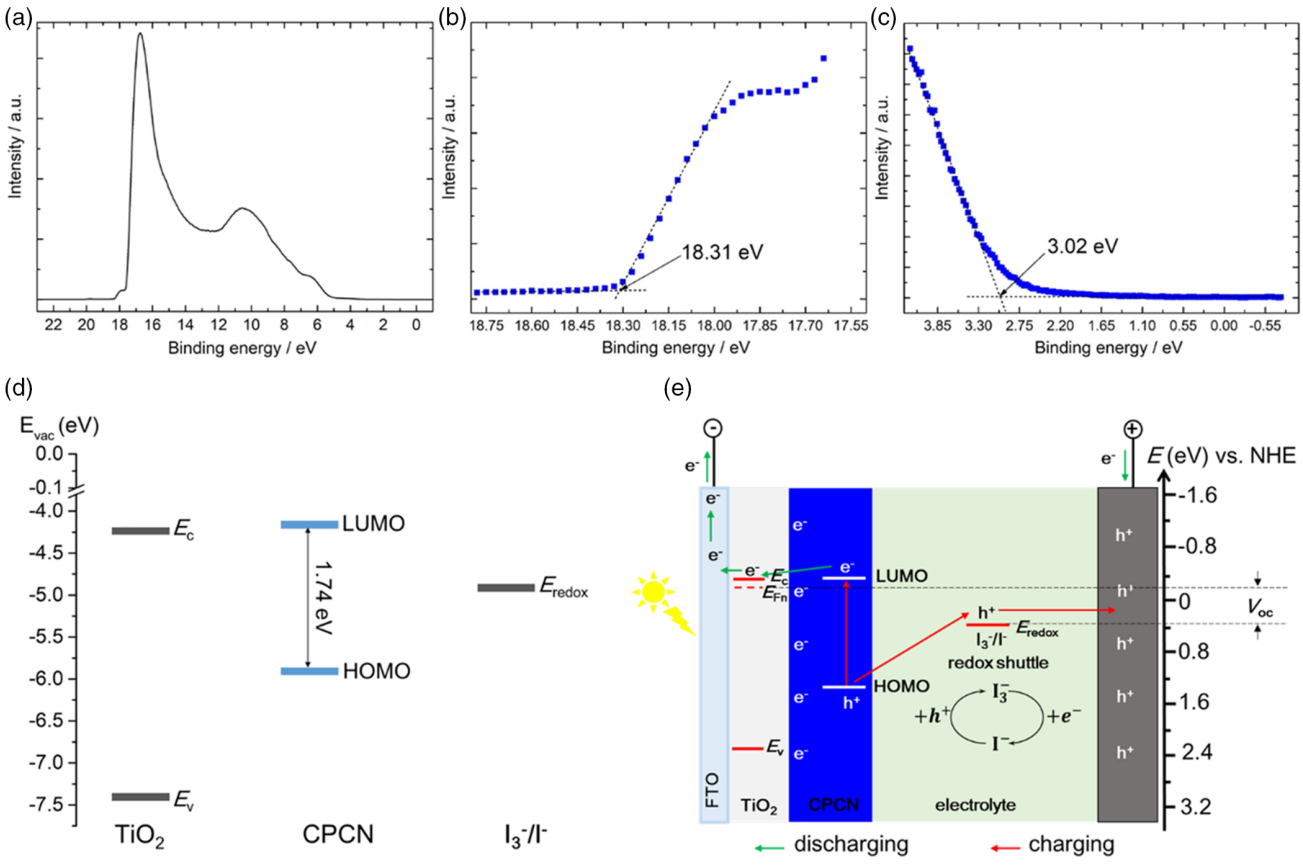

Figure 6. a) UPS survey spectrum, b) the secondary edge region, and c) the HOMO region of CPCN; d) schematic diagram for the energy levels of TiO_2 and CPCN, as well as the approximate redox potential (E_{redox}) of I_3^-/I^- in acetonitrile; e) schematics of the working mechanism of the light-induced charging and discharging in the CPCN-based cell.

illumination prolonged, most of photoelectrons were delayed to transport to the external circuit resulting in an effective charge storage.

To investigate the influence of light on the photoinduced charging and discharging performance of the CPCN-based cell, we ran the photoelectrochemical experiments under the condition of increasing the irradiance (mW cm^{-2}) gradually or altering the illuminating time.

Calculated from the CV curves tested under different irradiance (**Figure 7**a), the specific charge capacity of the cell increases linearly from 2.46 to 4.77 C g^{-1} as the irradiance increases from 30 to 190 mW cm^{-2} (Figure 7b). The higher light intensity (more

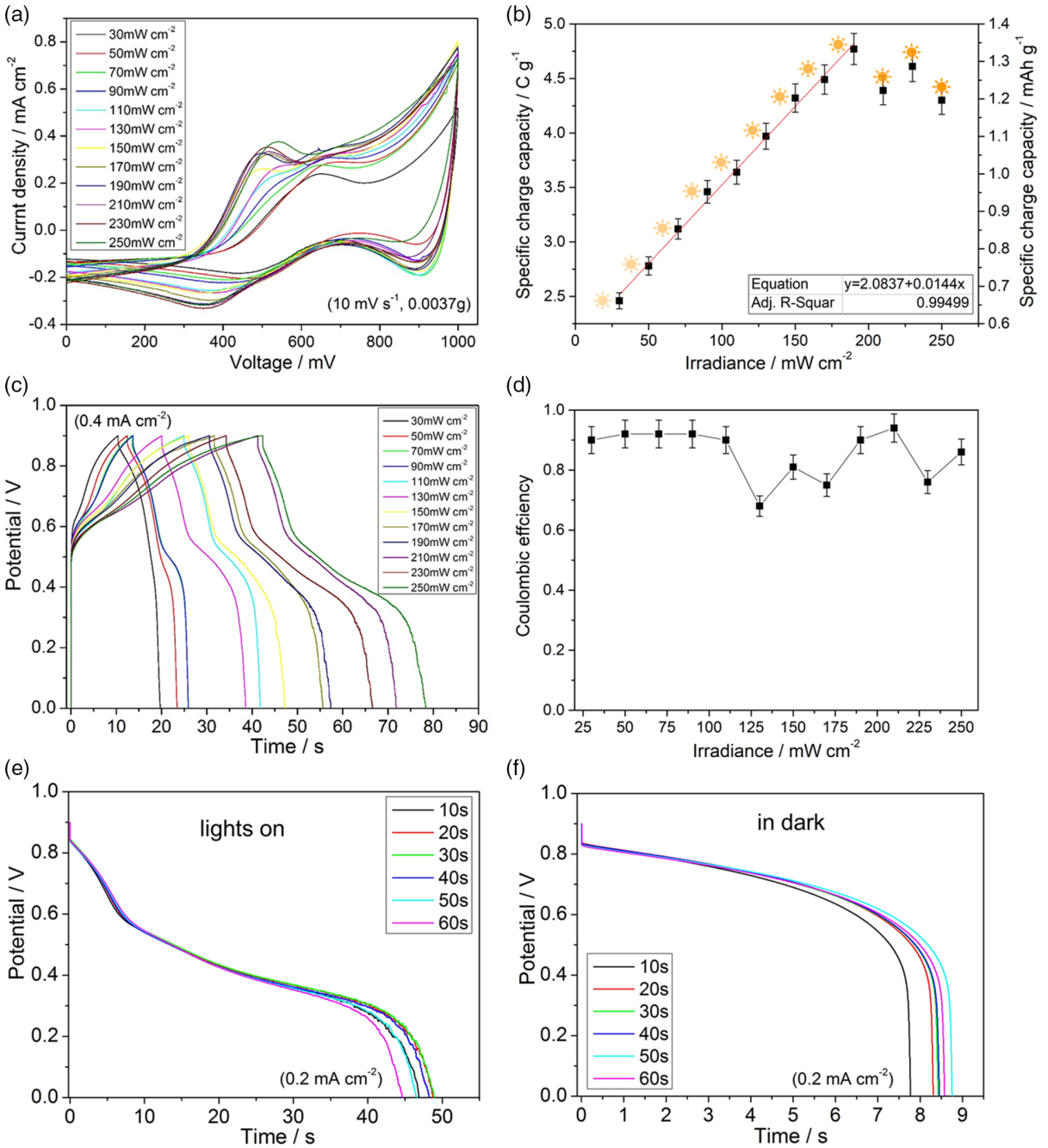

Figure 7. a) CV curves of the CPCN-based cell tested under the simulated solar irradiation with different irradiances (from 30 to 250 mW cm^{-2}), in a potential range of 0–1 V at the scan rates of 10 mV s^{-1}; b) specific charge capacity calculated from the CV curves; c) GCD tests under different irradiance at a current density of 0.4 mA cm^{-2} and in a potential window of 0–0.9 V; d) dependence of the irradiance on the coulombic efficiency (The CPCN loading on the photoelectrode is 0.0037 × g and the incident area of the photoelectrode is 0.25 cm^2.); discharging curves e) under illumination (150 mW cm^{-2}) or f) in dark after the cell being illuminated for different time under open-circuit conditions.

than 210 mW cm^{-2}) causes the capacity decreasing slightly. For a photoelectrode with a small incident area of 0.25 cm^2, the light-induced capacity keeping increasing till a high light intensity of about 200 mW cm^{-2} demonstrates a strong optical absorption of the light absorber (the dark blue CPCN) and an efficient photon-to-electron conversion of the system. The coulombic efficiency calculated from the GCD test of the cell (Figure 7c) is stable between 0.9 and 0.92 as the irradiance increases from 30 to 110 mW cm^{-2}, and fluctuates within 0.68–0.94 in the range of 130–250 mW cm^{-2} (Figure 7d). The discharging tests undertook after the cell being preirradiated for different time under open-circuit conditions. As the preirradiation time increased from 10 to 60 s, the discharging curves show no obvious difference, neither under illumination nor in dark, as shown in Figure 7e,f. This might result from that the light excitation and charge storage happened in one material and the light-induced charging behaved as a trigger effect.

3. Conclusion

In summary, a CPCN was synthesized by the hydrothermal method using citric acid and urea as the reactants followed with aging at room temperature over a month. The CPCN has a hybrid conjugated backbone of heptazine motifs and GR domains linked by bridging nitrogen in N—$(C)_3$ or H—N—$(C)_2$ group, which leads to a narrow bandgap of 1.74 eV and a unique morphology of 3D nanomeshes constructed by 2D networks. The photoelectrochemical solar cell fabricated using CPCN as the light absorber, TiO_2 as the electron transporter and I_3^-/I^- as the redox shuttle in electrolyte, successfully demonstrated the light-induced charge storage.

The CPCN material and the CPCN-based cell show some special properties, which are intriguing and their basic mechanisms are worthy of further study: 1) the bandgap tuning by introducing graphite domains and bridging nitrogen to expand the conjugation length of carbon nitrogen heterocycles; 2) the simultaneous photoconversion and charge storage in one material; 3) the irradiance-linearly-dependent but preirradiation time-independent capacity increasing properties, which suggests a potential development of ultrafast photocharging or photo-aid-charging devices. Although the performance of the CPCN cell is poor on its infant stage, it offers a significant opportunity to take its unique photoelectrochemical properties to realize direct photo to electric energy conversion and storage in one single material cell.

Supporting Information

Supporting Information is available from the Wiley Online Library or from the author.

Acknowledgements

L.H. and X.T. contributed equally to this work. Financial supports from the Venture & Innovation Support Program for Chongqing Oversea Returnee (grant no. CX2017023), the Construction of double city economic circle in Chengdu Chongqing region scientific and technological innovation project (grant no. KJCX2020028), the National Natural Science Foundation of China (grant no. 12004061) are acknowledged.

Conflict of Interest

The authors declare no conflict of interest.

Data Availability Statement

Research data are not shared.

Keywords

carbon nitrides, light-induced charge storage, photoelectric conversion, solar cells

Received: May 30, 2021
Revised: July 14, 2021
Published online: August 8, 2021

[1] B. Mortazavi, M. Makaremi, M. Shahrokhi, *Carbon* **2018**, *137*, 57.
[2] W. Xiong, M. Y. Huang, F. Huang, R. Q. Zhang, *Appl. Surf. Sci.* **2020**, *211*, 145535.
[3] Y. Hou, Z. Wen, S. Cui, *Adv. Mater.* **2013**, *25*, 6291.
[4] G. Algara-Siller, N. Severin, S.Y. Chong, *Angew. Chem., Int. Ed.* **2014**, *53*, 7450.
[5] T. Wang, C. Nie, Z. Ao, *J. Mater. Chem. A* **2020**, *8*, 485.
[6] F. Li, M. Tang, T. Li, *Appl. Catal., B* **2020**, 268.
[7] J. Safaei, N. A. Mohamed, M. F. M. Noh, *J. Mater. Chem. A* **2018**, *6*, 22346.
[8] Y. Yang, D. Yu, H. Wang, L. Guo, *Adv. Mater.* **2017**, 1703040.
[9] X. Tang, J. Qian, Z. Wang, H. Wang, Q. Feng, G. Liu, *J. Colloid Interface Sci.* **2009**, *330*, 386.
[10] Z. Li, S. Wu, J. Zhang, *Solar RRL* **2020**, *4*, https://doi.org/10.1002/solr.201900413.
[11] J. Liu, *Adv. Mater.* **2019**, 1901261.
[12] D. Kong, Y. Gao, Z. Xiao, *Adv. Mater.* **2018**, 1804973.
[13] M. Inagaki, T. Tsumura, T. Kinumoto, *Carbon* **2019**, *141*, 580.
[14] S. Qi, X. Ma, B. Yang, L. Sun, *Carbon* **2019**, *149*, 234.
[15] G. P. Mane, S. N. Talapaneni, K. S. Lakhi, H. Ilbeygi, U. Ravon, K. Al-Bahily, T. Mori, D. H. Park, A. Vinu, *Angew. Chem., Int. Ed.* **2017**, *56*, 8481.
[16] P. Kumar, E. Vahidzadeh, U. K. Thakur, *J. Am. Chem. Soc.* **2019**, *141*, 5415.
[17] S. N. Talapaneni, G. P. Mane, A. Mano, C. Anand, D. S. Dhawale, T. Mori, A. Vinu, *ChemSusChem* **2012**, *5*, 700.
[18] P. Zhang, X. Li, C. Shao, Y. Liu, *J. Mater. Chem. A* **2015**, *3*, 3281.
[19] X. Fang, R. Gao, Y. Yang, D. Yan, *iScience* **2019**, *16*, 22.
[20] P. Liu, L. Zhang, G. Liu, H. M. Cheng, *Adv. Funct. Mater.* **2012**, *22*, 4763.
[21] H. B. Zheng, W. Chen, H. Gao, Y.Y Wang, H.Y Guo, S.Q. Guo, Z.L Tang, *J. Mater. Chem. C* **2016**, *00*, 1.
[22] C. Chen, W. Cai, M. Long, B. Zhou, Y. Wu, D. Wu, Y. Feng, *ACS Nano* **2010**, *4*, 6425.
[23] Z. Zhang, F. Xiao, Y. Guo, S. Wang, Y. Liu, *ACS Appl. Mater. Interfaces* **2013**, *5*, 2227.
[24] Q. Yang, S. Yu, P. Fu, *Adv. Funct. Mater.* **2020**, 1910205.
[25] Z. Mo, H. Xu, Z. Chen, X. She, *Appl. Catal., B* **2019**, *241*, 452.
[26] F. Zheng, Y. Yang, Q. Chen, *Nat. Commun.* **2014**, 1.
[27] Y. Si, E. T. Samulski, *Nano Lett.* **2008**, *8*, 1679.
[28] F. Podjaski, J. Kröger, B. V. Lotsch, *Adv. Mater.* **2018**, 1705477.
[29] D. Geng, S. Yang, Y. Zhang, *Appl. Surf. Sci.* **2011**, *257*, 9193.
[30] C. Hu, Y. Liu, Y. Yang, *J. Mater. Chem. B* **2013**, *1*, 39.

[31] D. Usachov, O. Vilkov, A. Grüneis, *Nano Lett.* **2011**, *11*, 5401.
[32] J. Xu, F. Xu, M. Qian, *Adv. Mater.* **2017**, 1701674.
[33] S. Hou, X. Cai, H. Wu, *Energy Environ. Sci.* **2013**, *6*, 3356.
[34] I. Papailias, N. Todorova, *Appl. Catal. B* **2020**, *268*, 118733.
[35] X. Hua, X. Zenga, Y. Liu, *Appl. Catal. B* **2020**, *268*, 11846.
[36] H. J. Li, B.W. Sun, L. Sui, *Phys. Chem. Chem. Phys.* **2015**, *17*, 3309.
[37] W. J. Ong, L.L. Tan, S.P. Chai, *Nano Energy* **2015**, *13*, 757.
[38] G. Boschloo, A. Hagfeldt, *Chem. Res.* **2009**, *42*, 1819.
[39] S. Burnside, J.-E. Moser, K. Brooks, M. Grätzel, *J. Phys. Chem. B* **1999**, *103*, 9328.
[40] T. Daeneke, T. Kwon, A. B. Holmes, N. W. Duffy, U. Bach, L. Spiccia, *Nat. Chem.* **2011**, *3*, 211.
[41] L. Zheng, T. Zhu, W. Xu, L. Liu, J. Zheng, X. Gong, F. Wudl, *J. Mater. Chem. C* **2018**, *6*, 3634.
[42] S. Cao, J. Low, J. Yu, M. Jaroniec, *Adv. Mater.* **2015**, *27*, 2150.
[43] W. Ong, L. Tan, Y. H. Ng, S. Yong, S. Chai, *Chem. Rev.* **2016**, *116*, 7159.